Detecting Angle of Arrival on a Hybrid RIS Using Intensity-Only Data

Idban Alamzadeh, *Graduate Student Member, IEEE*, and Mohammadreza F. Imani, *Member, IEEE*

***Abstract*—Reconfigurable reflective metasurfaces—or reconfigurable intelligent surfaces (RISs)—can redirect incident signals toward desired directions, an ability that allows for sculpting wireless communication channels with desired characteristics. This smart radio environment, however, necessitates the information about the transmitter(s) and the receiver(s) to be available at the RIS. One possible solution to this need is to add sensing capability to the RIS. However, sensing complex wireless signals (i.e., both amplitude and phase) often requires complicated setups. In this letter, we propose and numerically demonstrate a reconfigurable reflective metasurface that uses intensity-only samples of the incident signal to retrieve desired information about the propagation environment. To do that, we will randomly tune the metasurface elements to multiplex information incident on all of them. The phaseless multiplexed data are then processed using computational ghost imaging algorithm to retrieve the desired information. As a demonstrative example, we present the detection of the incident angle from a user in a free-space environment. This simplified sensing process can pave the way for incorporation of RISs with integrated sensing capabilities in future wireless communication or sensing systems.**

***Index Terms*—Angle of arrival (AoA), ghost imaging (GI), metasurface.**

I. Introduction

ADAPTIVE wireless propagation environments empowered by reconfigurable intelligent surface (RIS) have garnered much interest recently [1], [2], [3], [4], [5], [6]. In these so-called smart radio environments, RISs redirect signals toward desired directions or realize over-the-air equalization [7], [8], [9], [10], [11], [12], [13], [14], [15], [16]. The RIS's promising attributes, however, strongly depend on the knowledge about the propagation environment, such as the incident signal's direction or intended reflection angle. Since RISs are ideally designed to reflect the signal (and not sense it), obtaining necessary information about the channel at the RIS elements has become a hindering challenge.

Over the years, several works have proposed solutions to this problem. A common approach is to use joint channel estimation [17], [18] using the information about the cascaded channel. This method, however, is computationally expensive since it aims to estimate separate channels from jointly sensed data. To overcome that, some have suggested adding dedicated sensing elements to the RIS [19] and applying compressive sensing. Dedicated antennas attached to a receiver would reduce the effective reflective aperture of the RIS and may disrupt the phase profile needed for forming desired reflection patterns. Alternatively, a novel RIS was proposed in [20] that can switch to an absorption mode; by comparing the received power in the absorption mode with an extensive look-up table for all possible angles of arrival (AoA), the incident angle can be found. Another method is to use AoA-dependent frequency shift in time-modulated RISs [21]. Similarly, the estimation of AoA has been demonstrated by applying time-domain orthogonal codes to the signals incident on the metasurface [22]. These approaches, however, require complicated metasurface configurations with time modulation and a dedicated receiving antenna connected to a receiver near the RIS. Alternatively, it is suggested in [23], [24], [25], [26], and [27] to use hybrid RISs (HRISs) that consist of hybrid meta-atoms: elements that can reflect the signal while also sense a portion of the incident signal. In particular, [23] and [28] have shown that using only a few such hybrid elements is enough to retrieve desired information about the channel. To do that, they used the HRIS in a novel manner where it realizes random multiplexing of the incident signal. By demultiplexing the signal collected in this manner, the desired features of the incident signal can be retrieved.

All the abovementioned methods require conventional sensing of complex data to deduce information about the incoming waves. Detecting complex signals (i.e., amplitudes and phases) necessitates complicated circuitry. If instead, intensity-only data can be used for detecting desired characteristics about the environment, the complexity of the receiving unit at the HRIS can be substantially reduced. While ABSense RIS [20] may in principle use intensity-only data, it requires a complicated search among many impedance profiles to match the incident signal impedance. Here, we are interested in a sensing protocol that does not require a complicated dictionary look-up process.

Toward this goal, we take inspiration from intensity-only computational microwave imaging, which has received a lot of attention over the last decade [29], [30], [31], [32]. In particular, the computational ghost imaging (GI) technique or coincidence imaging has recently been applied to intensity-only measurements to recover reflection patterns of a region of interest [32]. The underlying idea in these works is to use a dynamic metasurface antenna (DMA) that can generate a series of precharacterized spatially diverse patterns to illuminate a scene of interest. By

Manuscript received 5 April 2023; revised 6 June 2023; accepted 11 June 2023. Date of publication 21 June 2023; date of current version 6 September 2023. This work was supported by the National Science Foundation Award ECCS-2030068 under subaward 333-2727 to Arizona State University. *(Corresponding author: Idban Alamzadeh.)*

The authors are with the School of Electrical, Computer, and Energy Engineering, Arizona State University, Tempe, AZ 85287 USA (e-mail: amuham23@asu.edu; mohammadreza.imani@asu.edu).

Digital Object Identifier 10.1109/LAWP.2023.3288123

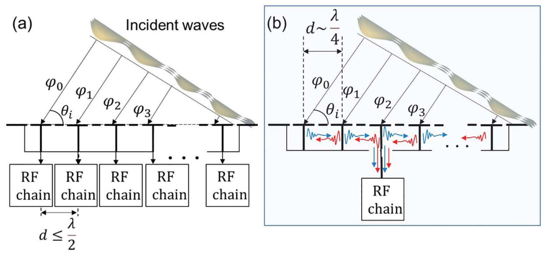

Fig. 1. Comparative depiction of (a) conventional sensing mechanism and (b) proposed sparse sensing mechanism for an RIS.

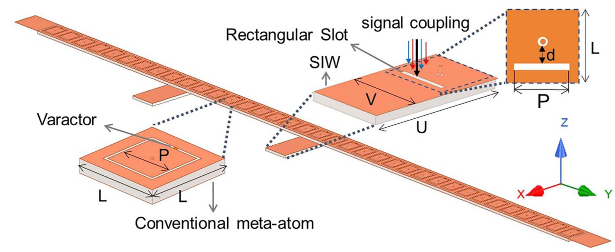

Fig. 2. Proposed HRIS architecture for intensity-only measurement. Here, $P = 8.1$ mm, $U = 35$ mm, $V = 17.5$ mm, $d = 3.7$, and $L = 13.1$ mm.

correlating the intensity of the return signal with the illuminating patterns, one can deduce the location of targets in the scene. Here, our goal is to leverage the GI principle to estimate the AoA on an HRIS.

In this letter, we update the compressive sensing architecture proposed in [28] to sense the incoming signal from only two sensing elements. The intensity of the difference of the signal captured by each of these elements is used for sensing purposes, eliminating the need for phase detection altogether. We then recast the computational GI method to be used for analyzing the intensity data. Using full-wave simulation, we show that the proposed intensity-only sensing operation can be used to detect the AoA of an incoming signal in free space.

II. Sparse Sensing of Phaseless Data

Recovering complex incident signals can overcomplicate an RIS configuration, outdoing the benefits it can bring to the network. This is especially the case if we connect circuitry for phase (and intensity) detection to each element of an RIS which typically can have hundreds of elements. Such a setup is shown schematically in Fig. 1(a). To circumvent this issue, previous works have suggested using compressive sensing of the incident wave from signal collected by a few receiving circuitry. Using a sparse array of receivers, one can reduce the spatial resolution of the detecting aperture. One solution to this problem, as suggested in [28], is to use multiplexing of the incident signal on all elements in the shared substrate of the elements, as shown in Fig. 1(b). This can be possible when elements of the HRIS exhibit random scattering responses. The multiplexed signal can then be processed to retrieve the incident signal on all elements. The only requirement is to obtain diverse measurements of the incident signal, which can be accomplished by using different multiplexing weights. In the case of [28], the varactors exciting each element is set randomly (we will refer to a configuration of varactor diodes as “masks” for brevity). In this manner, the signal coupled to the substrate from each element is randomly weighted, resulting in diverse measurements of the incident signal.

To realize this sensing protocol, one possible implementation is to use an HRIS with two different meta-atoms as shown in Fig. 2. This structure consists of well-known mushroom structures [33], each loaded with a varactor diode. To implement hybrid meta-atoms, as shown in Fig. 2, we add a rectangular slot to the ground plane of the mushroom structure. This slot also serves as an opening in the broad wall of a substrate-integrated waveguide (SIW). Using this slot, we can couple the signal in the shared substrate of the HRIS into the SIW [34], which guides the coupled signal toward sensing units [28]. The location and size of this opening were tailored to ensure that a sufficient amount of power is coupled to the SIW. The HRIS and the sensing SIWs are both implemented with a 1.52 mm thick Rogers 4003C substrate. The dimension, size, and composition of the hybrid meta-atom and the HRIS array are similar to the one in [28] as the operating frequency, 5.8 GHz, is the same. For completeness, these dimensions are denoted in Fig. 2. The design process to arrive at these values is presented in [28] and is not repeated here. As shown in [28], such a geometry can sense incident signals as well as redirect them toward desired directions. However, in contrast to [28], we only use two hybrid elements in this work. Our goal in this letter is to use this setup to retrieve relevant information about the channel (i.e., AoA) using only the intensity of the received signal.

When using intensity-only data, the inverse problem at the heart of AoA detection becomes much more complicated. To better illustrate this point, consider the case of two antennas tasked with detecting the AoA of an incident signal. By examining the phase difference between signals incident on the two antennas, i.e., the difference in measured phase, ϕ, in Fig. 1(a), one can detect AoAs. The intensity of the received signal on the antennas will, in fact, be almost identical. In other words, intensity-only data do not usually exhibit variation as a function of AoA. If instead, we combine the complex signals of the two antennas with random weights before measuring the intensity, the resulting intensity would depend on the phase of each signal and thus would change as a function of the AoA. When applying a similar idea to the HRIS, we note that the random multiplexing of the incident signals can happen naturally in the proposed HRIS configuration. Specifically, when the surface of the HRIS exhibits a random surface reactance, the signal incident on it scrambles inside. This scrambling of the signal manifests itself as a multiplexing of signals incident on all elements. The signal at the end of the SIWs can thus be described as a random weighted sum of signals incident on all elements—i.e., the captured signal contains information about all incident phases, ϕ, in Fig. 1(b). If we examine the intensity of such a received signal, it changes as a function of the incident AoA. One issue with the random weighted sum is that it reduces the dimensionality of the incident signal from all elements to a single measurement. To overcome that, inspired by compressive microwave imaging, we can use different random masks.

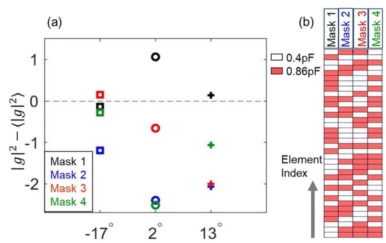

Fig. 3. (a) Intensity data for different AoAs. (b) Masks.

To demonstrate these points, we used the setup shown in Fig. 2 in Ansys HFSS. In our studies, we consider signals incident on the HRIS to be *X*-polarized plane waves in the *YZ*-plane. The goal of the sensing process is to deduce the AoA using only the intensity of the data. Similar to [28], we use binary masks where the varactor loading each element may randomly take one of the two different capacitive states of C1 = 0.4 or C2 = 0.86 pF. Following the same procedure as in [28], we use the signal difference between the two adjacent collecting waveguides. In practical implementation, the signal difference between the collecting waveguides can be formed using a 180° RF combiner. The intensity of the difference between the two signals can be sensed using a voltage or a power detector. Thus, only a single RF transmission line is required to pass the intensity data to a processor. The specific hardware layout for sensing is beyond the scope of this letter. Instead, we focus on demonstrating its possibility. Toward this goal, we take the intensity of the difference of the simulated signal at the end of each collecting waveguide numerically.

We denote the intensity of the difference signal obtained in the abovementioned manner with $|\mathbf{g}|^2$. This signal is plotted in Fig. 3(a) for different AoAs. We clearly see that the intensity of the signal changes as a function of the AoA, confirming that the intensity signals contain AoA-specific features. We have also plotted the signal intensity for different masks for each AoAs in Fig. 3(a). The random capacitance distribution corresponding to each mask is presented in Fig. 3(b). We clearly see that for the same AoA (denoted by the color), the phaseless data change as a function of masks, thereby validating the proposition to use random masks to diversify the data.

III. Computational GI

While the previous section illustrates the fact that intensity-only data are related to the AoA of the incident signal, we still need to formulate an algorithm to retrieve that information. In recent years, there has been a strong push to extend microwave imaging and sensing to phaseless detection [29], [30], [31], [32]. Various algorithms and hardware systems have been proposed for this purpose. In this work, inspired by the analogy of signal multiplexing in the proposed HRIS and that in DMAs in [32], we select to use computational GI. Yet, unlike the active imaging approach in [32], which relied on spatially diverse transmitted signals to retrieve reflectivity maps, our device does not transmit signals, instead, relies on the intensity of the incident signal.

To capture sufficient information for successful AoA estimation, we sense the incident signal multiple times using S random masks. Each sensed signal consists of the fields coupled to the hybrid meta-atoms and observed at the end of the SIWs attached to two hybrid meta-atoms. We denote these two field readings at the end of the SIWs as $\mathbf{g_1}$ and $\mathbf{g_2}$. For our studies, we examine the absolute difference between the two data streams. The final captured intensity $|\mathbf{g}|^2$ is then a real-valued vector, denoted as follows:

$$|\mathbf{g}|^2 = |\mathbf{g_1} - \mathbf{g_2}|^2 \in \mathbb{R}^S. \tag{1}$$

Following GI formulation, we subtract the ensemble average $\langle |\mathbf{g}|^2 \rangle$ from the intensity in (1), which yields the following:

$$\mathbf{I_g} = |\mathbf{g}|^2 - \langle |\mathbf{g}|^2 \rangle. \tag{2}$$

In this framework, AoA is determined based on the correlation of the collected intensity with a set of reference data. The reference data are comprised of a collection of known $\mathbf{I_g}$ for a set of preselected AoAs. Specifically, we used 25 AoAs uniformly distributed between $\pm 60°$ to construct the reference sensing matrix $\mathbf{H}$. In this manner, we discretize the continuous AoA range into 5° bins. The choice of the 120° sector around the normal direction is primarily based on the operation of RISs in practical settings since they cannot easily redirect beams to grazing angles without large sidelobes or grating lobes. It is worth mentioning that the HRIS can detect angles beyond $\pm 60°$ but with a lower resolution since its projected aperture is smaller for such angles. The 5° bins are used for two factors: 1) simulation time and 2) the HRIS's expected resolution. To ensure reasonable simulation time, we used a bin size that is the same as the beamwidth that would be generated by an array of the same size as the HRIS.

The simulated data for each of the reference AoAs are collected in the columns of $\mathbf{H}$. The estimated values are then determined from the cross-correlation between $\mathbf{I_g}$ and $\mathbf{H}$ as follows:

$$\mathbf{R_{IH}} = \frac{1}{S} \mathbf{I_g^*} \mathbf{H}. \tag{3}$$

The estimated parameter can then be related to the AoA in a similar manner as in [28]: the maximum of $\mathbf{R_{IH}}$ occurs at the bin center closest to the actual incident AoA. The correlation in (3) acts as a pattern matching parameter between the data of the incoming AoAs and the reference AoAs. Thus, the estimated AoA is the angle in $\mathbf{H}$ that has the highest correlation with $\mathbf{I_g}$. In other words, the AoA can be estimated from the maximum value given by (3).

It is important to note that the number of masks, S, may have a significant impact on the accurate estimation of the actual AoA. We thus begin our analysis by examining this factor. Toward this goal, we have plotted an illustrative example of the AoA detection process for a signal incident at 13° at 10 dB signal-to-noise ratio (SNR) in Fig. 4 as we increase the number of masks. We clearly see that using one mask or one measurement is not sufficient to detect the AoA. As we increase the number of masks, more diverse information is obtained and a better estimate is achieved. However, the increase in the amount of

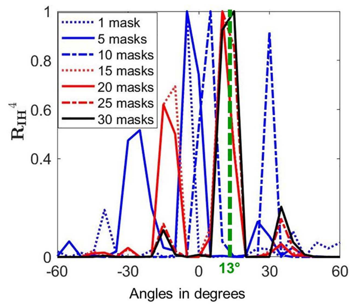

Fig. 4. Detecting a single AoA at 10 dB SNR for different numbers of masks. The dotted line represents the actual AoA, i.e., 13°.

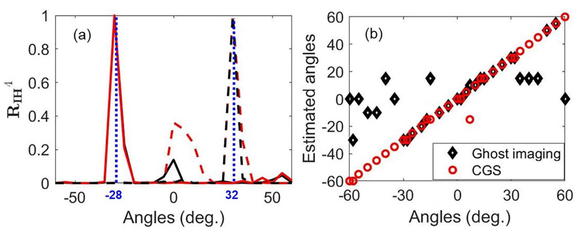

Fig. 5. (a) Detection of two different incident AoAs (superimposed with solid and dashed lines) using GI (black) and CGS (red). (b) Estimated AoAs for different incident AoAs.

information that newer masks provide starts to plateau. We can see from Fig. 4 that using around $S = 30$ masks should suffice for our purpose. We conducted this test for other AoAs (not shown here for brevity) and arrived at a similar conclusion.

Having set the required number of masks, we now examine how the performance changes for different AoAs with a few illustrations in Fig. 5(a). As expected, the maximum correlation occurs at the bin center closest to the test angle. In Fig. 5(b), we depict the estimated AoA for incident angles for the whole range of $\pm 60^\circ$. We clearly see that the estimated angles are close to the incident AoAs. However, the estimation fidelity degrades for angles that are farther from the normal (to some extent that is expected as the resolution degrades and larger bin sizes should have been used). By applying an iterative solver to the GI problem [e.g., conjugate gradient squared (CGS)], we can obtain accurate estimates for the whole $\pm 60^\circ$ range.

As explained in previous works on GI [31], [32], GI and coincident imaging are usually susceptible to the impact of noise. For example, the AoA detections presented in Fig. 5(a) and (b) are done with an SNR of 20 dB added to test signals $\mathbf{g_1}$ and $\mathbf{g_2}$. To better investigate the impact of noise, we compute the accuracy of the estimation as a function of noise. To do that, we note that our accuracy in detecting an AoA depends on the bin size (i.e., 5°) used to discretize the range of incident angles. With that in mind, we use a slightly larger bin size for setting the accuracy of detection since when the test AoA is halfway between two reference AoAs, either of the reference AoAs may be considered to be the estimated AoA with minimal degradation to the overall performance. Therefore, we consider an estimation within $\pm 3^\circ$ of the true AoA as accurate. Otherwise, the estimation is considered inaccurate. Thus, the estimation is a binary classification problem that assigns a value of 1 to an accurate estimation and 0 otherwise. We have calculated this accuracy for SNR values

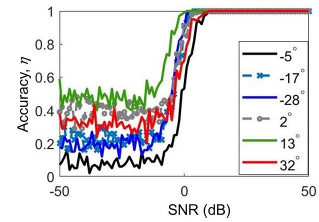

Fig. 6. Estimation accuracy for detecting various test AoAs.

of −50 to 50 dB. Because of the random nature of the noise, we averaged the accuracy calculation for each SNR value over 100 repetitions. A few illustrations of the accuracy calculations for a diverse set of AoAs are shown in Fig. 6. Evidently, the proposed GI technique can perform accurate AoA estimation with SNR values roughly larger than 0 dB. One can reduce the impact of noise by using more masks. Nonetheless, the results presented in Figs. 5 and 6 verify that we can detect AoA using only a single circuitry that measures the intensity at a single frequency. Lastly, we should note that the proposed HRIS can also realize the beamforming capabilities required for their use in smart radio environments. The beamforming results have been reported for various hybrid geometries before [23], [28], and are not reported here.

IV. Discussion

In summary, we investigated the problem of using intensity-only sparse data to retrieve relevant information about the propagation channel. We showed that using an HRIS with hybrid meta-atoms and multiplexing capabilities along with computational GI techniques provide a simple solution to this problem. Detecting signal strength or intensity requires a much simpler circuitry compared with other methods, which require retrieving phase information, paving the way for the widespread use of HRISs with sensing capabilities in wireless systems. An immediate future step is to extend this work to 2-D and demonstrate it in experiments. It is worth noting that we used binary reactive states to construct random masks in this letter. Thus, a potential way to further diversify the sensed data without increasing the number of masks would be to use more than two reactive states in a mask. Furthermore, as shown in previous works on computational imaging and sensing [35], [36], [37], the specific choice of masks and their distribution can impact the performance and one may reduce the number of required waveguides or masks by intelligently selecting those masks. Conducting such detailed studies on the choice of masks is left for future work. While we have used intensity data in the computational GI framework, one can instead utilize phase retrieval methods to obtain complete information about the channel [30], [38], [39]. It is worth noting that the proposed scheme is not frequency dependent and can easily be extended to higher frequencies by simple geometrical modifications to the RIS elements. The proposed configuration can also be used in applications other than wireless communication, e.g., in wireless power transfer systems to detect the location of the user, or in smart homes for detecting human presence or gesture recognition by processing intensity measurements from the electrically large aperture of HRIS.

REFERENCES

[1] E. Basar, M. Di Renzo, J. De Rosny, M. Debbah, M.-S. Alouini, and R. Zhang, "Wireless communications through reconfigurable intelligent surfaces," *IEEE Access*, vol. 7, pp. 116753–116773, 2019.

[2] C. Pan et al., "Reconfigurable intelligent surfaces for 6G systems: Principles, applications, and research directions," *IEEE Commun. Mag.*, vol. 59, no. 6, pp. 14–20, Jun. 2021.

[3] M. D. Renzo et al., "Smart radio environments empowered by reconfigurable AI meta-surfaces: An idea whose time has come," *EURASIP J. Wireless Commun. Netw.*, vol. 2019, no. 1, 2019, Art. no. 129.

[4] M. Di Renzo et al., "Smart radio environments empowered by reconfigurable intelligent surfaces: How it works, state of research, and the road ahead," *IEEE J. Sel. Areas Commun.*, vol. 38, no. 11, pp. 2450–2525, Nov. 2020.

[5] Q. Wu, S. Zhang, B. Zheng, C. You, and R. Zhang, "Intelligent reflecting surface-aided wireless communications: A tutorial," *IEEE Trans. Commun.*, vol. 69, no. 5, pp. 3313–3351, May 2021.

[6] E. Björnson, Ö. Özdogan, and E. G. Larsson, "Intelligent reflecting surface versus decode-and-forward: How large surfaces are needed to beat relaying?," *IEEE Wireless Commun. Lett.*, vol. 9, no. 2, pp. 244–248, Feb. 2020.

[7] N. Kaina, M. Dupré, G. Lerosey, and M. Fink, "Shaping complex microwave fields in reverberating media with binary tunable metasurfaces," *Sci. Rep.*, vol. 4, no. 1, pp. 1–8, 2014.

[8] P. Zivuku et al., "Maximizing the number of served users in a smart city using reconfigurable intelligent surfaces," in *Proc. IEEE Wireless Commun. Netw. Conf.*, 2022, pp. 494–499.

[9] M. F. Imani, S. Abadal, and P. D. Hougne, "Metasurface-programmable wireless network-on-chip," *Adv. Sci.*, vol. 9, no. 26, 2022, Art. no. 2201458.

[10] A. Araghi et al., "Reconfigurable intelligent surface (RIS) in the sub-6 GHz band: Design, implementation, and real-world demonstration," *IEEE Access*, vol. 10, pp. 2646–2655, 2022.

[11] M. A. ElMossallamy, H. Zhang, L. Song, K. G. Seddik, Z. Han, and G. Y. Li, "Reconfigurable intelligent surfaces for wireless communications: Principles, challenges, and opportunities," *IEEE Trans. Cogn. Commun. Netw.*, vol. 6, no. 3, pp. 990–1002, Sep. 2020.

[12] H. Zhang, N. Shlezinger, F. Guidi, D. Dardari, M. F. Imani, and Y. C. Eldar, "Beam focusing for near-field multi-user MIMO communications," *IEEE Trans. Wireless Commun.*, vol. 21, no. 9, pp. 7476–7490, Sep. 2022.

[13] P. D. Hougne, M. Fink, and G. Lerosey, "Optimally diverse communication channels in disordered environments with tuned randomness," *Nature Electron.*, vol. 2, no. 1, pp. 36–41, 2019.

[14] G. Lerosey and M. Fink, "Wavefront shaping for wireless communications in complex media: From time reversal to reconfigurable intelligent surfaces," *Proc. IEEE*, vol. 110, no. 9, pp. 1210–1226, Sep. 2022.

[15] J.-B. Gros, V. Popov, M. A. Odit, V. Lenets, and G. Lerosey, "A reconfigurable intelligent surface at mmWave based on a binary phase tunable metasurface," *IEEE Open J. Commun. Soc.*, vol. 2, pp. 1055–1064, 2021.

[16] G. C. Trichopoulos et al., "Design and evaluation of reconfigurable intelligent surfaces in real-world environment," *IEEE Open J. Commun. Soc.*, vol. 3, pp. 462–474, 2022.

[17] Z.-Q. He and X. Yuan, "Cascaded channel estimation for large intelligent metasurface assisted massive MIMO," *IEEE Wireless Commun. Lett.*, vol. 9, no. 2, pp. 210–214, Feb. 2020.

[18] L. Wei et al., "Joint channel estimation and signal recovery for RIS-empowered multi-user communications," *IEEE Trans. Commun.*, vol. 70, no. 7, pp. 4640–4655, Jul. 2022.

[19] Q. Ma et al., "Smart sensing metasurface with self-defined functions in dual polarizations," *Nanophotonics*, vol. 9, no. 10, pp. 3271–3278, 2020.

[20] C. Liaskos et al., "ABSense: Sensing electromagnetic waves on metasurfaces via ambient compilation of full absorption," in *Proc. Sixth Annu. ACM Int. Conf. Nanoscale Comput. Commun.*, 2019, pp. 1–6.

[21] J. Y. Dai et al., "Simultaneous in-situ direction finding and field manipulation based on space-time-coding digital metasurface," *IEEE Trans. Antennas Propag.*, vol. 70, no. 6, pp. 4774–4783, Jun. 2022.

[22] Q. Y. Zhou et al., "Two-dimensional direction-of-arrival estimation based on time-domain-coding digital metasurface," *Appl. Phys. Lett.*, vol. 121, no. 18, 2022, Art. no. 181702.

[23] I. Alamzadeh, G. C. Alexandropoulos, N. Shlezinger, and M. F. Imani, "A reconfigurable intelligent surface with integrated sensing capability," *Sci. Rep.*, vol. 11, no. 1, pp. 1–10, 2021.

[24] G. C. Alexandropoulos, N. Shlezinger, I. Alamzadeh, M. F. Imani, H. Zhang, and Y. C. Eldar, "Hybrid reconfigurable intelligent metasurfaces: Enabling simultaneous tunable reflections and sensing for 6G wireless communications," 2021, *arXiv:2104.04690*.

[25] H. Zhang et al., "Channel estimation with hybrid reconfigurable intelligent metasurfaces," *IEEE Trans. Commun.*, vol. 71, no. 4, pp. 2441–2456, Apr. 2023.

[26] J. He, A. Fakhreddine, and G. C. Alexandropoulos, "Joint channel and direction estimation for ground-to-UAV communications enabled by a simultaneous reflecting and sensing RIS," 2022, *arXiv:2210.15238*.

[27] R. Ghazalian, H. Chen, G. C. Alexandropoulos, G. Seco-Granados, H. Wymeersch, and R. Jäntti, "Joint user localization and location calibration of a hybrid reconfigurable intelligent surface," 2022, *arXiv:2210.10150*.

[28] I. Alamzadeh and M. F. Imani, "Sensing and reconfigurable reflection of electromagnetic waves from a metasurface with sparse sensing elements," *IEEE Access*, vol. 10, pp. 105954–105965, 2022.

[29] J. Laviada, A. Arboleya-Arboleya, Y. Alvarez-Lopez, C. Garcia-Gonzalez, and F. Las-Heras, "Phaseless synthetic aperture radar with efficient sampling for broadband near-field imaging: Theory and validation," *IEEE Trans. Antennas Propag.*, vol. 63, no. 2, pp. 573–584, Feb. 2015.

[30] O. Yurduseven, T. Fromenteze, D. L. Marks, J. N. Gollub, and D. R. Smith, "Frequency-diverse computational microwave phaseless imaging," *IEEE Antennas Wireless Propag. Lett.*, vol. 16, pp. 2808–2811, 2017.

[31] A. V. Diebold, M. F. Imani, T. Sleasman, and D. R. Smith, "Phaseless coherent and incoherent microwave ghost imaging with dynamic metasurface apertures," *Optica*, vol. 5, no. 12, pp. 1529–1541, 2018.

[32] A. V. Diebold, M. F. Imani, T. Sleasman, and D. R. Smith, "Phaseless computational ghost imaging at microwave frequencies using a dynamic metasurface aperture," *Appl. Opt.*, vol. 57, no. 9, pp. 2142–2149, Mar. 2018.

[33] D. Sievenpiper, L. Zhang, R. F. Broas, N. G. Alexopolous, and E. Yablonovitch, "High-impedance electromagnetic surfaces with a forbidden frequency band," *IEEE Trans. Microw. Theory Techn.*, vol. 47, no. 11, pp. 2059–2074, Nov. 1999.

[34] D. M. Pozar, *Microwave Engineering*, 4th ed. Hoboken, NJ, USA: Wiley, 2012.

[35] P. D. Hougne, M. F. Imani, A. V. Diebold, R. Horstmeyer, and D. R. Smith, "Learned integrated sensing pipeline: Reconfigurable metasurface transceivers as trainable physical layer in an artificial neural network," *Adv. Sci.*, vol. 7, no. 3, 2020, Art. no. 1901913.

[36] N. Viswanathan, S. Venkatesh, and D. Schurig, "Optimization of a sparse aperture configuration for millimeter-wave computational imaging," *IEEE Trans. Antennas Propag.*, vol. 69, no. 2, pp. 1107–1117, Feb. 2021.

[37] T. Fromenteze, O. Yurduseven, P. D. Hougne, and D. R. Smith, "Lowering latency and processing burden in computational imaging through dimensionality reduction of the sensing matrix," *Sci. Rep.*, vol. 11, no. 1, 2021, Art. no. 3545.

[38] E. J. Candes, X. Li, and M. Soltanolkotabi, "Phase retrieval via Wirtinger flow: Theory and algorithms," *IEEE Trans. Inf. Theory*, vol. 61, no. 4, pp. 1985–2007, Apr. 2015.

[39] B. Fuchs and L. Le Coq, "Excitation retrieval of microwave linear arrays from phaseless far-field data," *IEEE Trans. Antennas Propag.*, vol. 63, no. 2, pp. 748–754, Feb. 2015.